Improvement of Thermoelectric Performance of $CoSb_{3-x}Te_x$ Skutterudite Compounds by Additional Substitution of IVB-Group Elements for Sb

Wei-Shu Liu,[†,‡] Bo-Ping Zhang,[‡] Li-Dong Zhao,[†,‡] and Jing-Feng Li*[,†]

State Key Laboratory of New Ceramics and Fine Processing, Department of Materials Science and Engineering, Tsinghua University, Beijing 100084, China, and School of Materials Science and Engineering, University of Science and Technology Beijing, Beijing 100083, China

Received September 2, 2008. Revised Manuscript Received October 28, 2008

An enhanced ZT value as high as 1.1 at ~550 °C has been achieved in n-type nanostructured $CoSb_{3-x}Te_x$ skutterudite compounds through additional substitution of IVB-group elements (Si, Ge, Sn, Pb) for Sb. Particularly, Sn was found to be the most effective element to enhance the *ZT* value by extending the solubility limit of Te in $CoSb_{3-x}Te_x$, which decreases thermal conductivity more significantly than electrical conductivity. The reduced thermal conductivity is confirmed by the Raman scattering measurement of $CoSb_{2.86}M_{0.02}Te_{0.12}$ (M = Si, Ge, Sn, Pb), which shows that Ge and Sn enter into the Sb-site of $CoSb_3$ and generate significant changes in the vibration modes, whereas Si and Pb are not likely to get into the lattice of $CoSb_3$. Furthermore, nanostructure with fine grains and "nanodots" also contributes to the reduction of thermal conductivity.

Introduction

Thermoelectric energy conversion technique has received interests because of their promising application in directly converting both the existing heat in nature and waste heat generated in industry. However, the low efficiency limits their applications to some cases where reliability is more important than efficiency, such as space missions.[1] The efficiency of thermoelectric energy conversion is significantly controlled by the dimensionless figure of merit $ZT = T(\sigma\alpha^2)/\lambda$ of thermoelectric materials, where T is the absolute temperature, α the Seebeck coefficient, σ the electrical conductivity, and λ the thermal conductivity that is a sum of carrier component λ_{car} and lattice component λ_{lat}. However, the interdependence of these three physical parameters complicates the task of enhancing *ZT* value. An increase in σ usually leads to a decrease in α and an increase in λ_{car}. An introduction of phonon scattering mechanism to reduce λ_{lat} often simultaneously produces scattering on the electrons and hence decreases σ. Therefore, the challenge for the development of high-performance thermoelectric materials is to reduce λ_{lat} significantly while avoiding obvious deterioration of σ.[2,3]

Among many thermoelectric materials, $CoSb_3$-based skutterudites have received considerable interests because of their unique crystal structure and good thermoelectric properties.[4] There are two chemical approaches to enhance the thermoelectric performance of $CoSb_3$-based alloys: one is filling the lattice cage of skutterudite structure, and another is elemental substitution. Many studies so far have been conducted on filled $CoSb_3$ compounds, [5,6] which are limited to some specific filling elements and melting processing. As compared with filled $CoSb_3$-based alloys, there are more elements which can be used to substitute Co and/or Sb elements,[7,8] and most processes can be applied to its synthesis.[9−12] In our previous study,[13] the effect of Te substitution in $CoSb_3$ was confirmed, and a high $ZT \sim 0.9$ was achieved in nanostructured $CoSb_{3-x}Te_x$ fabricated by a powder metallurgy process combining mechanical alloying (MA) and spark plasma sintering (SPS). However, the solubility of Te in $CoSb_{3-x}Te_x$ is quite low (~5%) because of the charge difference between Te and Sb. This charge difference can be compensated by doping elements with less valence electron than host element Sb.

In this study, IVB-group elements (Si, Ge, Sn, Pb) were intentionally chosen as charge compensating element for Te

* Corresponding author. E-mail: jingfeng@mail.tsinghua.edu.cn.
† Tsinghua University.
‡ University of Science and Technology Beijing.

(1) Yang, J.; Caillat, T. *MRS Bull.* **2006**, *31*, 224.
(2) Dresselhaus, M. S.; Chen, G.; Tang, M. Y.; Yang, R. G.; Lee, H.; Wang, D. Z.; Ren, Z. F.; Fleurial, J. P.; Gogna, P. *Adv. Mater.* **2007**, *19*, 1043.
(3) Snyder, G. J.; Toberer, E. S. *Nat. Mater.* **2008**, *7*, 105.
(4) Uher, C. *Skutterudite: Prospective Novel Thermoelectrics in Recent Trends in Thermoelectric Materials Research I*; Tritt, T. M, Ed.; Semiconductors and Semimetals; Academic Press: San Diego, 2001; Vol. 69, p139.
(5) Chen, L. D.; Kawahara, T.; Tang, X. F.; Goto, T.; Hirai, T.; Dyck, J. S. W.; Chen, W.; Uher, C. *J. Appl. Phys.* **2001**, *90*, 1864.
(6) Nolas, G. S.; Kaeser, M.; Littleton IV, R. T.; Tritt, T. M. *Appl. Phys. Lett.* **2000**, *77*, 1855.
(7) Caillat, T.; Borshchevsky, A.; Fleurial, J. P. *J. Appl. Phys.* **1996**, *80*, 4442.
(8) Liu, W. S.; Zhang, B. P.; Li, J. F.; Zhang, H. L.; Zhao, L. D. *Acta Phys. Sin.* **2008**, *57*, 3791.
(9) Tang, X. F.; Chen, L. D.; Goto, T.; Hirai, T.; Yuan, R. Z. *Acta Phys. Sin.* **2000**, *49*, 1120.
(10) Toprak, M. S.; Stiewe, C.; Platzek, D.; Williams, S.; Bertini, L.; Müller, E.; Gatti, C.; Zhang, Y.; Rowe, M.; Muhammed, M. *Adv. Funct. Mater.* **2004**, *12*, 1189.
(11) Liu, W. S.; Zhang, B. P.; Li, J. F.; Zhao, L. D. *J. Phys. D: Appl. Phys.* **2007**, *40*, 6784.
(12) Liu, W. S.; Zhang, B. P.; Li, J. F.; Zhao, L. D. *J. Phys. D: Appl. Phys.* **2007**, *40*, 566.
(13) Liu, W. S.; Zhang, B. P.; Li, J. F.; Zhang, H. L.; Zhao, L. D. *J. Appl. Phys.* **2007**, *102*, 103717.

10.1021/cm802367f CCC: $40.75
Published on Web 12/03/2008

to raise the solubility of Te in $CoSb_{3-x}Te_x$. We found that a high ZT of 1.1 at 550 °C was achieved in the Sn/Te-co-doped $CoSb_3$ because of the significant decrease in lattice thermal conductivity but slight decrease in carrier mobility. The mechanism for improving the thermoelectric performance of $CoSb_3$ alloys by mixed elemental substitution for the Sb site has been discussed on the basis of the Raman scattering measurements and nanostructure observation experiments.

Experimental section

Synthesis. In the $CoSb_{3-y-x}M_yTe_x$ family, both n-type and p-type samples can be obtained by tuning the parameters x and y. In this study, two series of n-type $CoSb_{3-x}M_yTe_x$ (one is M = Sn, $y = 0.25 - x$, $x = 0.125, 0.150, 0.175, 0.200$; other is M = Si, Ge, Sn, Pb, $y = 0.02$, $x = 0.12$) samples were focused. The fabrication process used was similar to that reported in our previous studies.[8,13] A stoichiometric powder mixtures of Co, Sb, Te, and M (including Si, Ge, Sn, Pb) were subjected to mechanical alloying for 15 h at 450 rpm, and then sintered at 500 °C for 5 min by using a SPS system (Sumitomo SPS1050, Japan) under 50 MPa.

X-ray Diffraction Pattern. The phase constitutions were characterized by X-ray diffraction instrument (XRD, Rigaku2500, Cu Kα, Japan), which was operated at 40kV and 20mA. Lattice constant of $CoSb_3$ phase was determined from the data in the range of 2θ between 20° and 100° by an analytical extrapolation function of $(\cos^2\theta/\sin\theta + \cos^2\theta/\theta)/2$.

Field-Emission Scanning Electron Microscopy. The microstructure and chemical homogeneity of the samples were examined by field emission scanning electron microscopy (FE-SEM, JSM-6301F, Japan). Specimens used for the investigation are fixed on the copper holder by silver paste to avoid the specimen drift during the energy dispersive X-ray (EDX) measurement process.

High-Resolution Transmission Electron Microscopy. The nanostructure of some samples was examined using transmission electron microscopy (TEM, JSM-2011, Japan). Specimens used for the investigation were polished to about 50−60 μm with sand paper and subsequently diamond paste. Specimens were then thinned to electron transparency using a Gatan model 600CDIF precession ion-milling system at low angle (10−12°). HRTEM images of several different locations of the specimens were obtained at 200 kV.

Thermoelectric Transport Property. The Seebeck coefficient and electrical resistivity were measured using a Seebeck Coefficient/Electrical Resistivity Measuring System (ZEM-2, Ulvac-Riko, Japan). The thermal conductivity was calculated by the relationship of $\lambda = DC_pd$, where D, C_p, and d are the thermal diffusivity, heat capacity, and density, respectively. The thermal diffusivity D was measured by the laser flash method (Netzsch Laser Flash Apparatus LFA 427, Germany), and the density was measured by Archimedes method. The heat capacity used in this study is calculated data of pure $CoSb_3$,[14] which is given in the Supporting Information. The room-temperature heat capacity of doped $CoSb_3$ compounds were also confirmed using a differential scanning calorimeter (Dupont 1090B, USA). The experimental heat capacities are consistent with the calculated data, showing a little contribution by the composition change.

Raman Scattering Spectroscopy. To identify the effect of the group IV elements on the vibration modes, we investigated the Raman scattering response of $CoSb_{2.86}M_{0.02}Te_{0.12}$ (M = Si, Ge, Sn, Pb) samples. The room-temperature Raman scattering measurements were performed by using a microconfocal Raman spectrometer (RM2000, Reishaw, England). The laser excitation used was 514.5 nm line of an Ar^+-ion laser with a typical laser spot size of 2 μm. The Raman scattering data was collected by using a charge coupled device detector array with a typical resolution of 1.7 wave numbers.

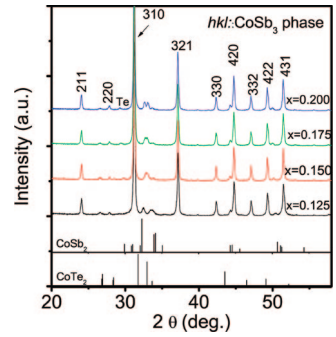

Figure 1. XRD patterns of $CoSb_{2.75}Sn_{0.25-x}Te_x$ ($x = 0.125$ 0.150, 0.175, 0.200). The standard data of $CoSb_2$ and $CoTe_2$ are referenced from the JCPDS Card Nos. PDF 65-4102 and PDF 89-2091, respectively.

Results and Discussion

Phase and Microstructure. Figure 1 shows the XRD patterns of $CoSb_{2.75}Sn_{0.25-x}Te_x$ ($x = 0.125, 0.150, 0.175, 0.200$). The XRD patterns demonstrate that the major phase is $CoSb_3$ phase, which is crystallized in a cubic $CoAs_3$-type structure with *IM*-3 space group. A small amount of $CoSb_2$ and $CoTe_2$ were also observed, which is similar to the previous case in $CoSb_{3-x}Te_x$,[13] but no diffraction peak of SnTe was detected. The XRD peaks of impurity slightly deviated from standard XRD patterns of $CoSb_2$ (PDF No. 65−4102) and $CoTe_2$ (PDF No. 89−2091), which is caused by the fact some Te/Sn atoms entered into the impurity phases. Takizawa et al. [15] reported that group IV elements, including Si, Ge, Sn and Pb, can enter into the cagelike 2*a* site of $CoSb_3$ lattice under a ultrahigh pressure of several GPa, which can be judged by the decreased ratio of (211)/(310) of XRD patterns. However, no such changes were observed in the present samples. In contrast, a p-type semiconductor was obtained as the concentration of Sn was much more than that of Te. The group IVB elements are likely to enter into the Sb-occupying *8c*-site rather than the cagelike *2a* site. The lattice constant increased almost linearly from ~9.0350 Å for pure $CoSb_3$ to 9.0413, 9.0428, 9.0433, and 9.0452 Å, respectively for $x = 0.125$, 0.150, 0.175, and 0.200 compositions, suggesting that additional Te atoms exceeding the solubility limit ($x = \sim 0.150$) in $CoSb_{3-x}Te_x$ successfully entered into the Sb-site of $CoSb_3$ lattice due to the coaddition of Sn. It is known that the doping solubility is affected by both the size difference and charge difference. The valence electron number (atom size) is 4 (1.72 Å), 5 (1.53 Å), 6 (1.42 Å), respectively, for Sn, Sb, Te. The addition of Sn not only compensates for the charge difference, but also relaxes the lattice stress due to the size difference between Te and Sb in $CoSb_{3-x}Te_x$. We also noted that the lattice constant of $CoSb_{3-x}Te_x$ was slightly decreased

(14) Barin, I. *Thermochemical Data of Pure Substrate (in Chinese)*; China Science Press: Beijing, 2003.

(15) Takizawa, H.; Miura, K.; Ito, M.; Suzuki, T.; Endo, T. *J. Alloys Compd.* **1999**, *282*, 79.

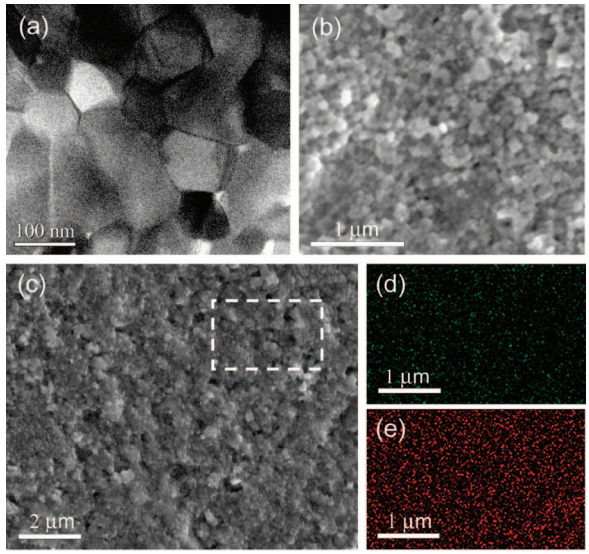

Figure 2. Microstructure and elemental distribution of the $CoSb_{2.75}Sn_{0.05}Te_{0.20}$ sample: (a) TEM image, (b) FE-SEM image, (c) EDX detecting region, (d) distribution of element Sn, and (e) distribution of element Te.

due to the additional substitution by Sn. For example, the lattice constant for $CoSb_{2.85}Te_{0.15}$ is 9.0447 Å,[13] whereas it is 9.0428 Å for $CoSb_{2.75}Sn_{0.01}Te_{0.15}$. At present, it is not well understood why the lattice constant of $CoSb_3$ increased when doped with smaller Te than Sb but decreased when doped with larger Sn, but such an abnormal change may be related to the special lattice structure of $CoSb_3$.

Figure 2 shows a representative microstructure and elemental distribution in submicro scale for the $CoSb_{2.75}Sn_{0.05}Te_{0.2}$ sample. We can see well-developed angular grains and clear grain boundaries from the TEM image (Figure 2a) and FE-SEM image (Figure 2b). The present average grain size is about 140 nm, which is slightly smaller than that (160 nm) of $CoSb_{2.85}Te_{0.15}$.[13] Such a fine-grained microstructure, which is in favor of thermoelectric materials requiring low thermal conductivity, was obtained because MA can produce fine particles, whose growth is subsequently suppressed during the SPS consolidation process. In order to investigate the chemical homogeneity of Sn/Te doped $CoSb_3$, we mapped the elemental distributions of $CoSb_{2.75}Sn_{0.05}Te_{0.2}$ by EDX, within an area shown in Figure 2c, and it was confirmed that the elemental distributions of Co, Sn, Sb, Te are homogeneous at submicro resolution. Figures 2d and 2e show the elemental distribution of Sn and Te in a small area as indicated by the white rectangle in Figure 2c.

Electrical Property. The temperature dependences of electrical resistivity and Seebeck coefficient of $CoSb_{2.75}Sn_{0.25-x}Te_x$ (x = 0.125, 0.150, 0.175, 0.200) were shown in Figure 3. Except for the sample with $x = 0.125$ showing semiconductor-like behavior, all other samples display semimetal-like character, showing positive temperature dependence on electrical resistivity. The electrical resistivity of $CoSb_{2.75}Sn_{0.25-x}Te_x$ decreases with increasing Te concentration. Because of the charge compensating effect of Sn, it is considered that only the Te atoms uncompensated by Sn could give out a free electron to contribute to the

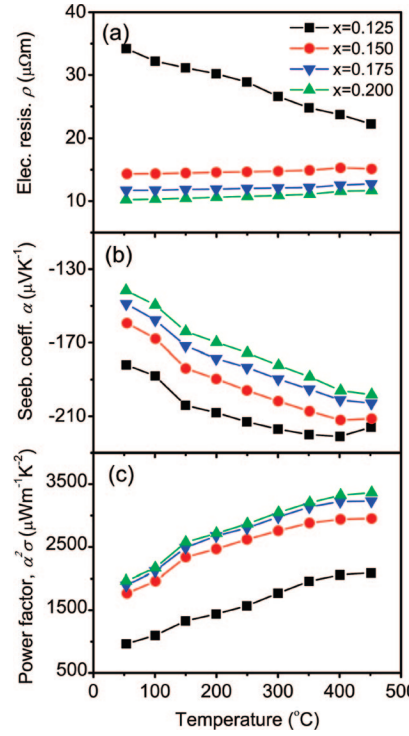

Figure 3. Temperature dependence of thermoelectric transport properties for the samples $CoSb_{2.75}Sn_{0.25-x}Te_x$ (x = 0.125 0.150, 0.175, 0.200): (a) electrical resistivity, (b) Seebeck coefficient, (c) power factor.

electric transport, and the carrier concentration of $CoSb_{2.75}Sn_{0.05}Te_{0.20}$ was comparable with $CoSb_{2.85}Te_{0.15}$. However, the room temperature electrical resistivity of $CoSb_{2.75}Sn_{0.05}Te_{0.20}$ (10.2 $\mu\Omega$m) is slightly higher than that observed in $CoSb_{2.85}Te_{0.15}$ (9.5 $\mu\Omega$m).[13] This may be caused by the fact that more lattice distortions in $CoSb_{2.75}Sn_{0.05}Te_{0.20}$ than that in $CoSb_{2.85}Te_{0.15}$, which generates stronger scattering against the electron, and hence resulting in low mobility.

Seebeck coefficient measurements conducted up to 450 °C revealed that all the samples were n-type in the whole temperature range (see Figure 2b). Regardless of composition, the absolute value of Seebeck coefficient (/α/) for $CoSb_{2.75}Sn_{0.25-x}Te_x$ increases almost linearly with temperature. The highest /α/ near room temperature is ~182 μV K^{-1} for the sample with $x = 0.125$, which increases almost linearly to ~221 μV K^{-1} at 400 °C. As T > 400 °C, /α/ tends to a maximum and then decreases, indicating the onset of intrinsic conduction. With increasing Te content, the extrinsic electron concentration increases while the intrinsic hole decreases originating from the cross-gap excitation.[13] As a result, the peak of /α/ shifts toward high temperature with increasing Te content. The temperature-dependent power factor curve shows that the sample with more Te has higher power factor, as shown in Figure 2c. The sample $CoSb_{2.75}Sn_{0.05}Te_{0.20}$ shows the highest power factor of 3300 μW m^{-1} K^{-2} at 450 °C. We also measured the thermoelectric properties of this sample up to ~550 °C, which showed a higher power factor of 3350 μW m^{-1} K^{-2} at 546 °C. This value is slightly lower than the value of 3540 μW m^{-1} K^{-2} at 547 °C obtained in $CoSb_{2.85}Te_{0.15}$.[13]

By solving Boltzmann transport equation of electron in a parabolic single-band approximate and a nondegenerate

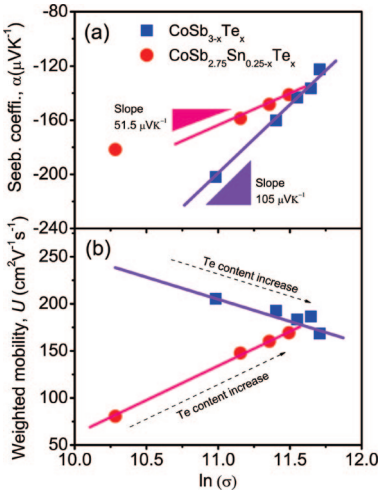

Figure 4. Seebeck coefficient (a) and weighted mobility (b) at room temperature as a function of natural logarithm electrical conductivity for the present samples $CoSb_{2.75}Sn_{0.25-x}Te_x$ (x = 0.125 0.150, 0.175, 0.200) and the previous samples $CoSb_{3-x}Te_x$ (y = 0, 0.05, 0.10, 0.15, 0.20) from ref 13.

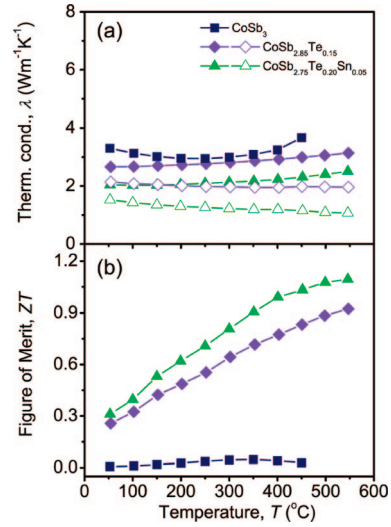

Figure 5. Temperature dependence of (a) total thermal conductivity (filled symbols) and lattice thermal conductivity (unfilled symbols) and temperature dependence of (b) figure of merit for the sample $CoSb_{2.75}Sn_{0.05}Te_{0.20}$. The date of pure $CoSb_3$ from ref 12 and $CoSb_{2.85}Te_{0.15}$ from ref 13 are also given for comparison.

approximate, Seebeck coefficient and electrical conductivity of n-type semiconductors can be expressed as,[16]

$$\alpha = -\frac{k_B}{e}\left[\left(s+\frac{5}{2}\right)-\xi\right] \quad (1)$$

$$\sigma = 2e\left(\frac{2\pi m_o k_B T_o}{h^2}\right)^{3/2}\left(\frac{T}{T_o}\right)^{3/2}(m^*/m_o)^{3/2}\mu \exp(\xi) \quad (2)$$

where h, ξ, s, T_o, and m_o are the Plank constant, reduced Fermi energy, scattering factor, room temperature and free electron mass, respectively. We can then express the Seebeck coefficient as a function of natural logarithm electrical conductivity

$$\alpha = -\frac{k_B}{e}\left[A+\frac{3}{2}\ln\left(\frac{T}{T_o}\right)+\ln U-\ln\sigma\right] \quad (3)$$

where A is scattering factor related parameter which is equal to 17.71 + s, U is weighted mobility which is defined as $(m^*/m_o)^{3/2}\mu$. The detailed derivation and validity discussion of eq 3 are given out in the Supporting Information. According to eq 3, for a given system with different Fermi energy, the value $\partial\alpha/\partial\ln(\sigma)$ should be a classic value k_B/e ($\sim$86.2 μV K^{-1}). Figure 4a plots the room temperature Seebeck coefficient of present samples $CoSb_{2.75}Sn_{0.25-x}Te_x$ and previously reported samples $CoSb_{3-x}Te_x$[13] as a function of natural logarithm electrical conductivity. Taking the slope of scattering data, we arrive at $\partial\alpha/\partial\ln(\sigma) \approx 105$ μV K^{-1} for the $CoSb_{3-x}Te_x$ samples, and $\partial\alpha/\partial\ln(\sigma) \approx 51.5$ μV K^{-1} for the $CoSb_{2.75}Sn_{0.25-x}Te_x$ samples. Both values significantly deviated from the classic result of $\partial\alpha/\partial\ln(\sigma)\sim k_B/e$, where k_B is the Boltzmann constant and e is the charge of electron. This fact indicates that the carrier effective mass m^* or carrier mobility μ is considerably affected by doping. By using eq 3, we estimate the transport parameter U from the measured Seebeck coefficient and electrical resistivity, as shown in Figure 4b. Here, acoustic phonon scattering is taken as the main carrier scattering mechanism, which has been extensively accepted in $CoSb_3$ based materials.[7] At first glance, the U values of $CoSb_{4-x}Te_x$ serial samples are higher than that of $CoSb_{2.75}Sn_{0.25-x}Te_x$ serial samples. The highest U value is 202 cm^{2}V^{-1}s^{-1} in $CoSb_{2.95}Te_{0.05}$, which is comparable to $m^* \approx 2.5m_0$ and $\mu \approx 50$ cm^2 V^{-1} s^{-1}.[7] With increasing ln σ or increasing Te content, the U decreases for the $CoSb_{3-x}Te_x$ compositions while increases for the $CoSb_{2.75}Sn_{0.25-x}Te_x$ samples. The U decreases in $CoSb_{3-x}Te_x$ because of the increased lattice disturbance by Te doping. However, in the $CoSb_{2.75}Sn_{0.25-x}Te_x$, the total doping content is the same (i.e., (Te + Sn)/Sb = 0.25/2.75), U shows a significant dependence on the ratio of Sn/Te. This fact indicates that the point defect Sn_{Sb} scatters more strongly the transport of electrons than the point defects Te_{Sb}. Here, the symbols Sn_{Sb} and Te_{Sb} mean that atoms Sn and Te occupy the Sb site in $CoSb_3$ lattice, respectively. Sn has less valence electron than Sb, whereas Te has more electron than Sb. As a result, the point defect Sn_{Sb} in $CoSb_3$ lattice is positive and easily absorbs the free electron and hence produces strong scattering.

Thermal Conductivity and *ZT* Value. Figure 5 displays the thermal conductivity and thermoelectric figure of merit for $CoSb_{2.75}Sn_{0.05}Te_{0.20}$ as a function of temperature. The data of two fine-grained samples $CoSb_3$[12] and $CoSb_{2.85}Te_{0.15}$[13] fabricated by MA-SPS method in our previous studies were also presented for comparison. It is noted that both samples $CoSb_3$ and $CoSb_{2.85}Te_{0.15}$ have fine grains ($\sim$160 nm) and hence lower thermal conductivity than the bulk materials with similar composition but large grain size (several micrometers). The thermal conductivity of $CoSb_{2.75}Sn_{0.05}Te_{0.2}$ is significantly lower than that of $CoSb_{2.85}Te_{0.15}$ in the whole measured temperature range, as shown in Figure 5a. At room temperature, the thermal conductivity of $CoSb_{2.75}Sn_{0.05}Te_{0.20}$ is 2.04 Wm^{-1}K^{-1}, which is much lower than that of $CoSb_{2.85}Te_{0.15}$ (2.66 W m^{-1} K^{-1}). It is well-known that the bipolar diffusive thermal conductivity (λ_{bip}) is significant for

(16) Nolas, G. S.; Sharp J.; Goldsmid, H. J. *Thermoelectrics: Basic Principles and New Materials Developments*; Springer: New York, 2001.

the narrowing semiconductor, especially at high temperature or low doping level. According to our previous study, [13] the $\lambda_{bip}/\lambda_{tot}$ is estimated to be only 2.5% for the $CoSb_{2.85}Te_{0.15}$ because of the high extrinsic carrier. By considering electric charge compensation of Te by Sn, the donor doping level of $CoSb_{2.75}Sn_{0.05}Te_{0.20}$ is comparable to that of $CoSb_{2.85}Te_{0.15}$. Therefore, we estimated λ_{lat} by subtracting λ_{car} from λ_{tot}, as indicated by unfilled symbols in Figure 5a. Here, λ_{car} can be estimated by Wiedemann−Franz's law, $k_{car} = LT/\rho$, where L is calculated to be 1.7×10^{-8} V^2 K^{-2}. Because the difference in λ_{car} between $CoSb_{2.75}Sn_{0.05}Te_{0.20}$ (0.445 W m^{-1} K^{-1} at 50 °C) and $CoSb_{2.85}Te_{0.15}$ (0.518 W m^{-1} K^{-1} at 50 °C) is quite small, the reduction in thermal conductivity is mainly contributed to by the decreased λ_{lat} because of the enhancement of point defect scattering. The present sample $CoSb_{2.75}Sn_{0.05}Te_{0.20}$ has similar grain size and density with previous sample $CoSb_{2.85}Te_{0.15}$, but its lattice thermal conductivity is significantly reduced. The thermal conductivity of $CoSb_3$-based material can be considerably decreased by including mass fluctuation through doping other atoms,[7,8] by reducing grain size due to the grain boundary scattering,[10,12] or by combining both scattering effects.[7,13] The low thermal conductivity of present $CoSb_{2.75}Sn_{0.05}Te_{0.20}$ is a result of combining the grain boundary scattering and the point defect scattering. Since the electric charge compensation of Sn atoms, the solubility limit of Te in $Co(Sb, Sn)_{3-x}Te_x$ is shifted from $x = 0.15$ to $x = 0.20$. The amount of mass fluctuation in $CoSb_{2.75}Sn_{0.05}Te_{0.20}$ is higher than that in $CoSb_{2.85}Te_{0.15}$.

According to the measured electrical resistivity, Seebeck coefficient, and thermal conductivity, the *ZT* values were calculated and plotted as a function of temperature in Figure 5b. The *ZT* values of $CoSb_{2.75}Sn_{0.05}Te_{0.20}$ are higher than that of $CoSb_{2.85}Te_{0.15}$ in the whole measured temperature range (50−550 °C) because of significantly decreased lattice thermal conductivity. The maximum *ZT* value of $CoSb_{2.75}Sn_{0.05}Te_{0.20}$ is 1.1 at ∼550 °C, which is about 10-fold higher than the maximum of pure $CoSb_3$. This value is also comparable to many state-of-the-art filled $CoSb_3$ compounds.[4−6]

Phonon Scattering Mechanism. As compared with $CoSb_{2.85}Te_{0.15}$, the enhanced *ZT* in $CoSb_{2.75}Sn_{0.05}Te_{0.20}$ is mainly due to the significant decrease in lattice thermal conductivity while slight decrease in electrical conductivity. From the viewpoint of point defect scattering, it sounds reasonable because the sample $CoSb_{2.75}Sn_{0.05}Te_{0.20}$ have much more mass fluctuations than the sample $CoSb_{2.85}Te_{0.15}$. We also try to explore the deeper reasons from the viewpoints of the change in vibration mode and the difference in nanostructure nature. Figure 6 shows the Raman shift of $CoSb_{2.86}M_{0.02}Te_{0.12}$ (M = Sb, Si, Ge, Sn, Pb). According to the theoretical calculation,[17] there are eight Raman sensitive phonon vibration modes in $CoSb_3$, identified as $2A_g + 2E_g + 4F_g$, with six appeared in the wavenumber ranges from 100 to 225 cm^{-1}. Five of six modes were observed in our Raman scattering measurements. Since the theoretical F_{g4} mode (178 cm^{-1}) and A_{g2} mode (179 cm^{-1}) are so close that we were unable to distinguish them. As M = Sb, i.e., for the $CoSb_{2.88}Te_{0.12}$ sample, the peaks at 134.4, 150.2, 176.5, and 183.5 cm^{-1} were observed, which are in good agreement with the theoretical predication. The highest-frequency vibration mode shows the highest Raman response intensity, which is inconsistent with Nolas et al.'s observation.[18] We believe that this mode should be the E_{g2} vibration mode, which is related with the out-of-phase motion between two Sb_4 rings. The samples $CoSb_{2.86}Si_{0.02}Te_{0.12}$ and $CoSb_{2.86}Pb_{0.02}Te_{0.12}$ display similar Raman response patterns to $CoSb_{2.88}Te_{0.12}$, whereas the samples $CoSb_{2.86}Ge_{0.02}Te_{0.12}$ and $CoSb_{2.86}Sn_{0.02}Te_{0.12}$ show significant changes. The most notable change is the shift of peaks toward the low-frequency. Koyanagi et al.[19] reported that Sb in $CoSb_3$ can be partially substituted by Ge and Sn but not by Pb. Therefore, we deduced that Si and Pb did not enter into the Sb site because of the large atomic size difference, while Ge and Sn got into the Sb site and generated considerable disturbance of vibration mode. In the theoretical Raman vibration modes of $CoSb_3$, the wavenumber distances of F_{g3}, F_{g4}, and A_{g2} from E_{g2} are 25, 4, and 3 cm^{-1}, respectively. Surprisingly, a "new" peak at ∼167.3 cm^{-1} was observed in both $CoSb_{2.86}Ge_{0.02}Te_{0.12}$ and $CoSb_{2.86}Sn_{0.02}Te_{0.12}$, which have ∼11 cm^{-1} from the E_{g2} vibration model (∼178.3 cm^{-1}). This possibly resulted from the shift by one of the F_{g3}, F_{g4}, and A_{g2} modes, or the splitting of one degenerate vibration mode because of the broken symmetry of Sb_4 rings as Sn, Te, or both Sn and Te enter into the Sb_4 rings. The effect of point defect scattering on the thermal conductivity can be understood by the significant changes in the vibration modes.

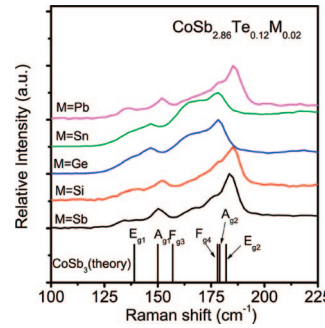

Figure 6. Raman shift of the samples $CoSb_{2.86}M_{0.02}Te_{0.12}$ (M = Sb, Si, Ge, Sn, Pb). The data of theoretically calculated modes for $CoSb_3$ from ref 17 are also presented.

We also noted that the $CoSb_{3-y-x}M_yTe_x$ (M = Ge, Sn) family can be considered as an alloy between binary compound $CoSb_3$ and ternary compound that have a general formula $AM_{1.5}Te_{1.5}$.[20−22] The quaternary compound $CoSb_{3-y-x}M_yTe_x$ is very analogous to the $AgPb_mXTe_{m+2}$ (X = Sb, Bi) system, which is also thought of as an alloy of PbTe and $AgXTe_2$.[23] One of the predominant features in $AgPb_mSbTe_{m+2}$ systems is the presence of quantum "nano-

(17) Feldman, J. L.; Singh, D. J. *Phys. Rev. B* **1996**, *53*, 6273.
(18) Nolas, G. S.; Kendziora, C. A.; Takizawa, H. *J. Appl. Phys.* **2003**, *94*, 7440.
(19) Koyanagi, T.; Tsubouchi, T.; Ohtani, M.; Kishimoto, K.; Anno H.; Matsubara. K. *Proceedings of the 15th International Conference on Theromoelectrics*, Pasadena, CA, March 26−29, 1996; Institute of Electrical and Electronics Engineers: Piscataway, NJ, 1996; p 107.
(20) Nolas, G. S.; Yang, J.; Ertenberg, R. W. *Phys. Rev. B* **2003**, *68*, 193206.
(21) Bos, J. W. G.; Cava, R. J. *Solid State Commun.* **2007**, *141*, 38.
(22) Vaqueiro, P.; Sobany, G. G.; Stindl, M. *J. Solid State Chem.* **2008**, *181*, 768.

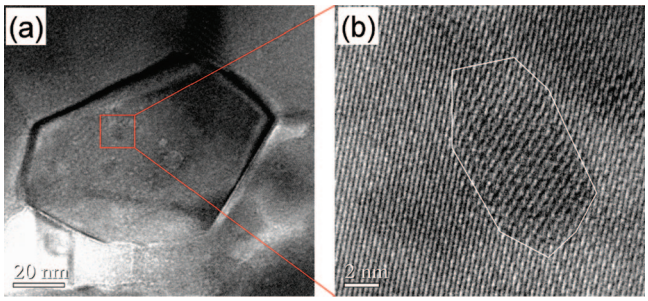

Figure 7. Nanostructure in the single grain of the sample $CoSb_{2.75}Sn_{0.05}Te_{0.20}$: (a) a panorama of a grain, (b) a possible "nanodot".

dots" through a melting and slow cooling method.[24,25] Wang et al.[26] also observed nanosized inhomogenous region in their bulk material fabricated MA-SPS method. The fabrication process of $CoSb_{2.75}Sn_{0.05}Te_{0.20}$ investigated is similar to that used by Wang et al.. We also expected that a similar microstructure should be observed. Figure 7 shows high resolution TEM images of the $CoSb_{2.75}Sn_{0.05}Te_{0.20}$ sample. A few nanoscopic black regions embedded in the matrix, as shown in Figure 7a. As seen from Figure 7b, the high-resolution TEM image confirmed the character of "nanodot" observed in the $AgPb_{18}XTe_{20}$ (X = Sb, Bi) system.[24−27] Therefore, these "nanodots" would scatter phonon transport and were responsible for the low thermal conductivity of $CoSb_{2.75}Sn_{0.05}Te_{0.20}$ besides the point defect scattering and the grain boundary scattering.

Conclusions

The solubility limit of Te in $CoSb_{3-x}Te_x$ is increased by additional substitution of IVB-group elements as electric-charge compensation. It was found that the thermal conductivity (electrical resistivity) of $CoSb_{2.75}Sn_{0.05}Te_{0.20}$ is much lower (slight higher) than that of $CoSb_{2.85}Te_{0.15}$. An enhanced *ZT* value as high as 1.1 at ~550 °C was therefore obtained in $CoSb_{2.75}Sn_{0.05}Te_{0.20}$. The Raman scattering measurement of $CoSb_{2.86}M_{0.02}Te_{0.12}$ (M = Si, Ge, Sn, Pb) indicates that Ge and Sn enter into the Sb site of $CoSb_3$ and generate significant changes in the vibration modes, whereas Si and Pb are not likely to get into the Sb site of $CoSb_3$. This notable change in atomic vibration mode can be used to explain the effect of point defect scattering against the thermal conductivity. A few "nanodots" similar to that observed in $Ag_{1-x}Pb_mSbTe_{m+2}$ exist, which are also responsible for the low thermal conductivity.

Acknowledgment. This work was supported by National Basic Research Program of China (Grant Nos. 2007CB607504 and 2007CB607505) and Natural Science Foundation of Beijing (Grant 2072009).

Supporting Information Available: Calculated heat capacity of pure $CoSb_3$, the derivation detail of weight mobility formula, the validity and possible error of weight mobility formula (PDF). This material is available free of charge via the Internet at http://pubs.acs.org.

CM802367F

(23) Kanatzidis, M. G. The Role of Solid-State Chemistry in the Discovery of New Thermoelectric Materials. In *Recent Trends in Thermoelectric Materials Research I*; Tritt, T. M., Ed.; Semiconductors and Semimetals; Academic Press: San Diego, 2001; Vol. 69; p 51.
(24) Hsu, K. F.; Loo, S.; Guo, F.; Chen, W.; Dyck, J. S.; Uher, C.; Hogan, T.; Polychroniadis, E. K.; Kanatzidis, M. G. *Science* **2004**, *303*, 818.
(25) Han, M. K.; Hoang, K.; Kong, H.; Pcionek, R.; Uher, C.; Paraskevopoulos, K. M.; Mahanti, S. D.; Kanatzidis, M. G. *Chem. Mater.* **2008**, *20*, 3512.
(26) Wang, H.; Li, J. F.; Nan, C. W.; Zhou, M.; Liu, W. S.; Zhang, B. P.; Kita, T. *Appl. Phys. Lett.* **2006**, *88*, 092104.
(27) Zhou, M.; Li, J. F.; Kita, T. *J. Am. Chem. Soc.* **2008**, *130*, 4527.